Supporting Information

Nano-wired Polyaniline/VS_2 Composite Materials for All-solid-state Supercapacitor and Zinc-ion Battery Applications

Saad Zafar, Santosh K. Singh, and Bimlesh Lochab**

[a]*Department of Chemistry, School of Natural Sciences, Shiv Nadar Institution of Eminence, Delhi-NCR-201314*

*Bimlesh Lochab

Materials Chemistry Laboratory, Department of Chemistry, School of Natural Sciences, Shiv Nadar Institution of Eminence, Delhi-NCR-201314, India

Email: bimlesh.lochab@snu.edu.in

*Santosh K. Singh

Electrochemical Energy Laboratory, Department of Chemistry, School of Natural Sciences, Shiv Nadar Institution of Eminence, Delhi-NCR-201314, India

Email: santosh.singh1@snu.edu.in

Table of content:

Experimental details for surface area and pore size distribution. The BET surface area and pore volume were determined by using nitrogen adsorption/desorption isotherms at 77.35 K on Quantachrome analyzer. All samples were degassed for 6 h at 150 °C prior to analysis. BET surface area was measured using the BET (Brunauer–Emmett–Teller) method in relative pressure range of P/P_o (0.05–0.3) and total pore volume (V_t) was taken at P/P_o = 0.99. Total micropore area (S_{micro}), external surface area (S_{ext}), and micropore volume (V_{micro}) were determined using *t*-plot method. Mesopore volume was calculated as the difference of total pore volume (V_t) and micropore volume (V_{micro}). The mesoporous nature of the material is further confirmed by the experimental determination using the Barrett–Joyner–Halenda (BJH) pore size distribution curves.

Micropore area and micropore volume were calculated from de Boer's linear thickness plot (*t*-plot).

Thickness of the adsorbed layer of N_2 was calculated according to de Boer's equation:

$$\text{Thickness of adsorbent (in Å)} = 0.88(P/P_0)^2 + 6.45(P/P_0) + 2.98 \qquad \text{Equation (S1a)}$$

According to de Boer's formula,

$$\text{Micropore area} = \text{slope} \times 15.47 \qquad \text{Equation S1b}$$

$$\text{Micropore volume} = \text{intercept} \times 0.001547 \qquad \text{Equation S1c}$$

From the desorption curve, $1/[W(P_o/P) - 1)]$ *vs* P/P_o linear plot was obtained. *'W'* is the weight of adsorbate (N_2) per unit mass of adsorbent. The value of *'W'* was derived from sorbed volume of N_2 (V), Density of N_2 (0.808 g L^{-1}) and weight of the adsorbate taken.

Specific surface area was calculated from the linear plot of $1/[W(P_o/P) - 1)]$ vs P/P_o.

$$W_m = \frac{1}{Slope + Intercept} \qquad \text{Equation S2a}$$

Where, W_m = Weight of the adsorbate as monolayer

$$\text{Total Surface Area, } S_{total} = \frac{W_m . N_A . A_{CS}}{M} \qquad \text{Equation S2b}$$

N_A = Avogadro Number, A_{CS} = Cross sectional area of the adsorbate (16.2 $Å^2$ mol^{-1} for N_2), M = MW of Adsorbate (28.013 g mol^{-1} for N_2)

$$\text{Specific Surface Area, S} = \frac{S_{total}}{W} \qquad \text{Equation S2c}$$

W = Weight of the adsorbent taken

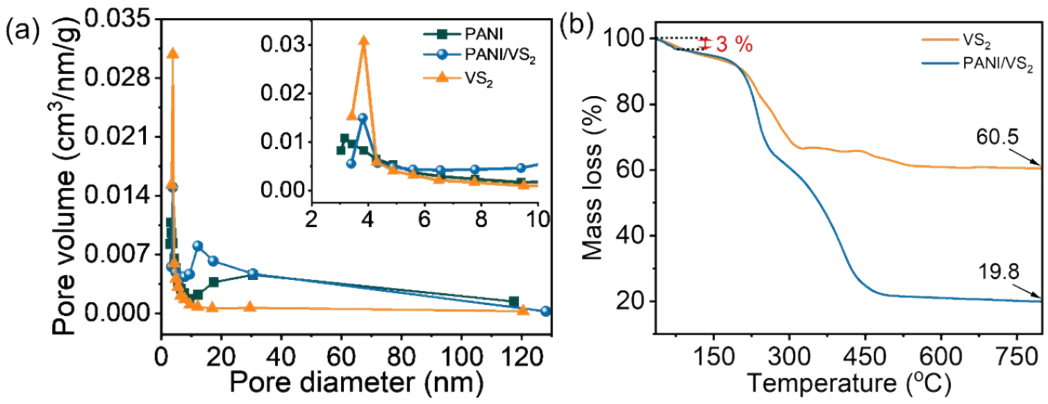

Figure S1. (a) BJH pore size distribution curve of PANI, PANI/VS_2 and VS_2 composite (b) TGA curve of VS_2 and PANI/VS_2.

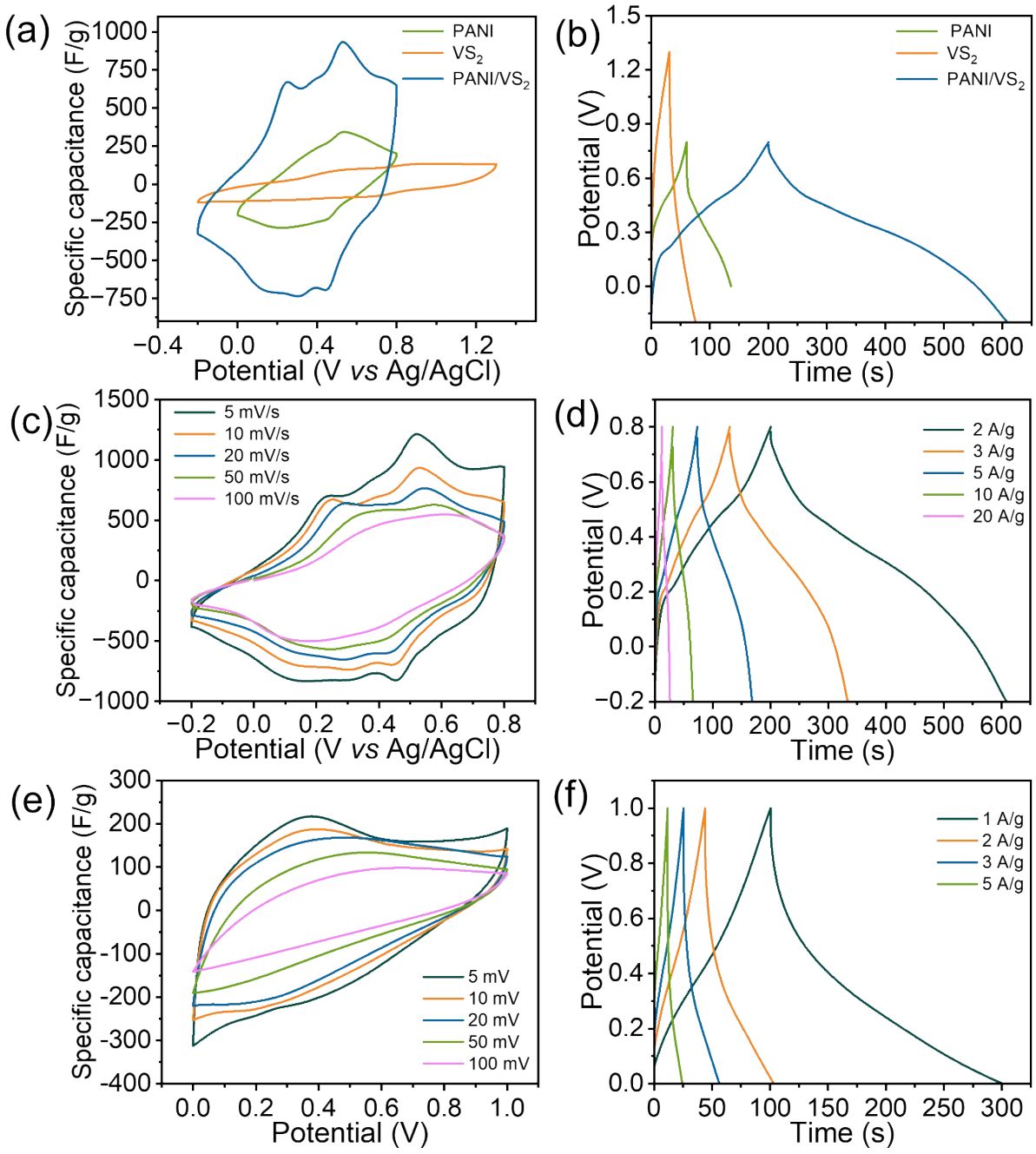

Figure S2. Electrochemical performances in 0.5 M H_2SO_4 electrolyte. (a) CV curves for PANI, VS_2, and PANI/VS_2 samples at a scan rate of 10 mV/s, (b) GCD curves at the current density of 2 A g^{-1}, (c) CV curves of PANI/VS_2 in three electrodes from 5 mV s^{-1} to 100 mV s^{-1} (d) GCD curves of PANI/VS_2 in three-electrode from 2 A g^{-1} to 20 A g^{-1}, (e) CV curves of PANI/VS_2 in two-electrode from 5 mV s^{-1} to 100 mV s^{-1}, and (f) GCD curves of PANI/VS_2 in two-electrode from 1 A g^{-1} to 5 A g^{-1}.

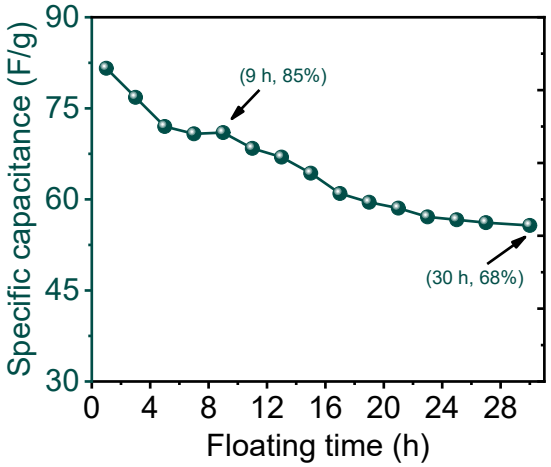

Figure S3. Floating test as a function of capacitance at 1 A g^{-1}. Test experiment with 5 GCD cycles and 2 h of voltage holding till 15 cycles. The floating test analysis of the QSSC device shows ~68% retention in the specific capacitance after the durability test.

(a) (b)

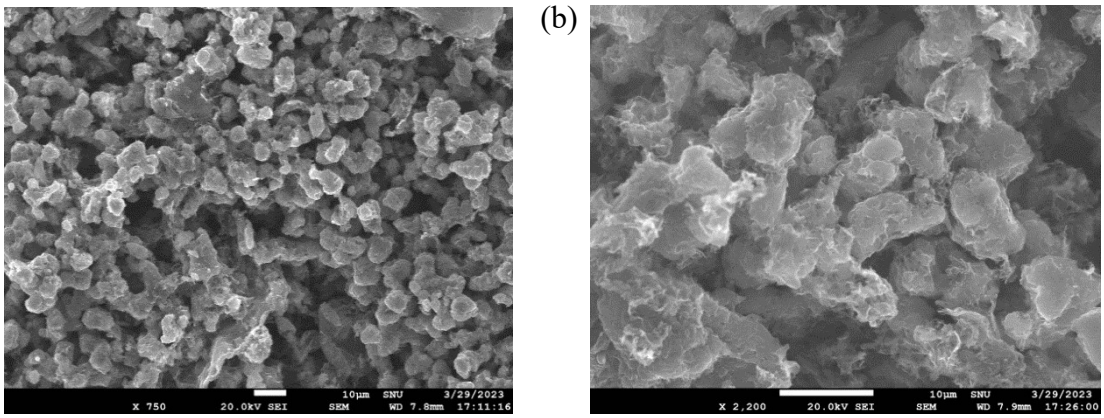

Figure S4. Post-mortem SEM analysis of the QSSC device after 500 cycles (a) low and (b) high resolution image. An agglomeration of the active materials is observed.

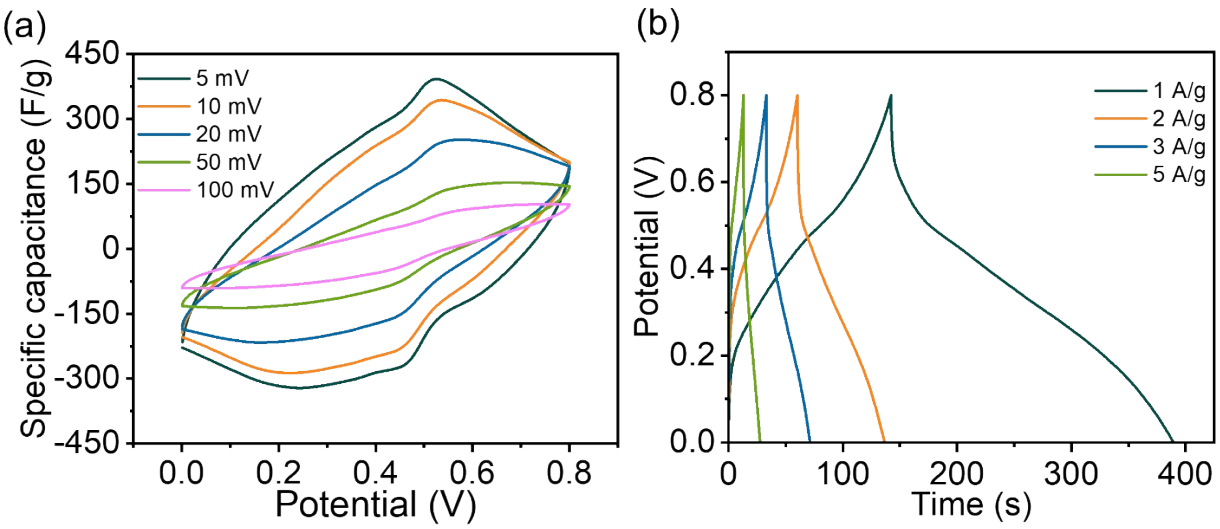

Figure S5. Electrochemical performance of PANI in 0.5 M H_2SO_4 electrolyte. (a) CV curves at different scan rates, and (b) GCD curves at different current density.

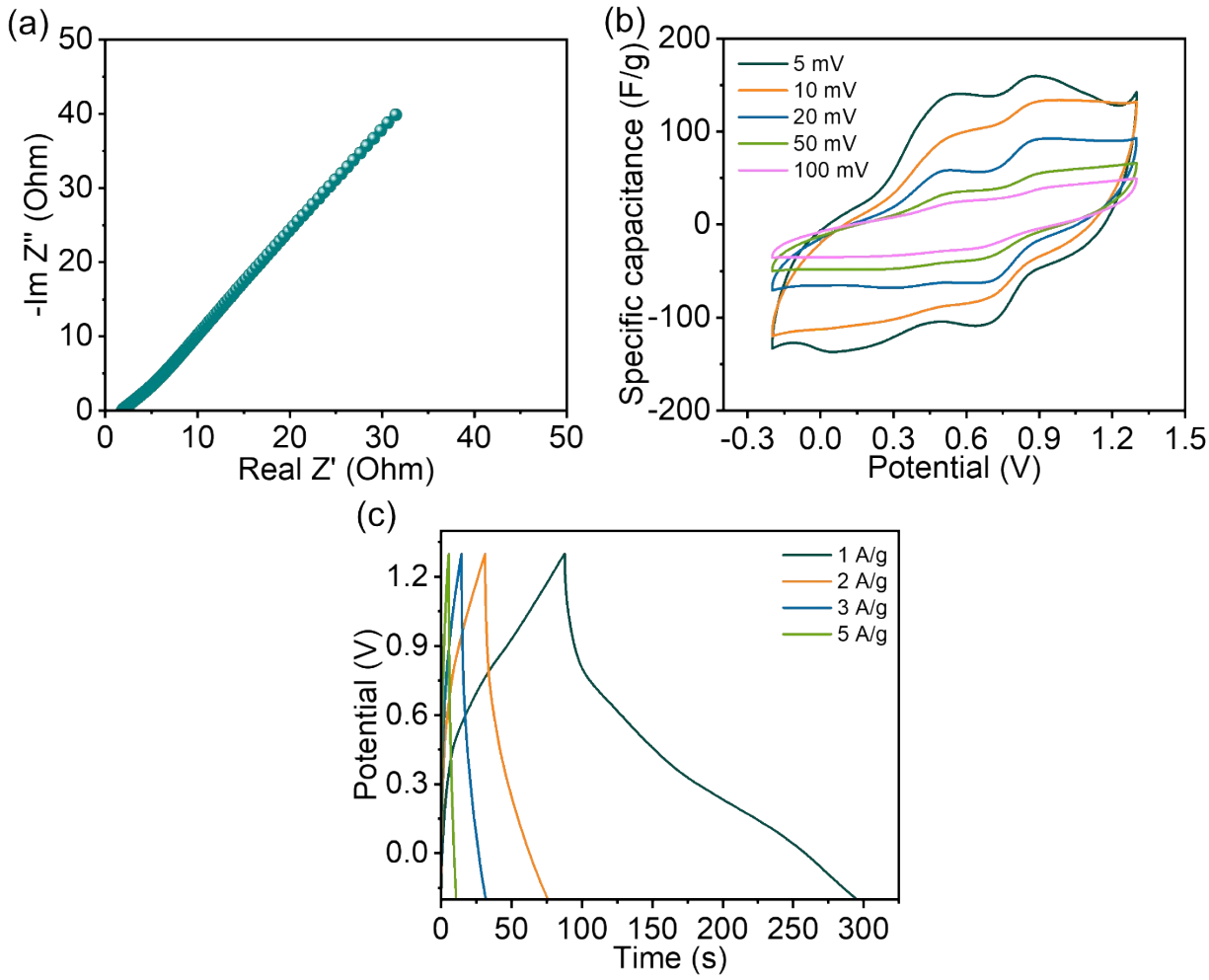

Figure S6. Electrochemical performance of VS_2 in a three-electrode system, (a) EIS impedance, (b) CV curves at different scan rates, and (c) GCD curves at different current density.

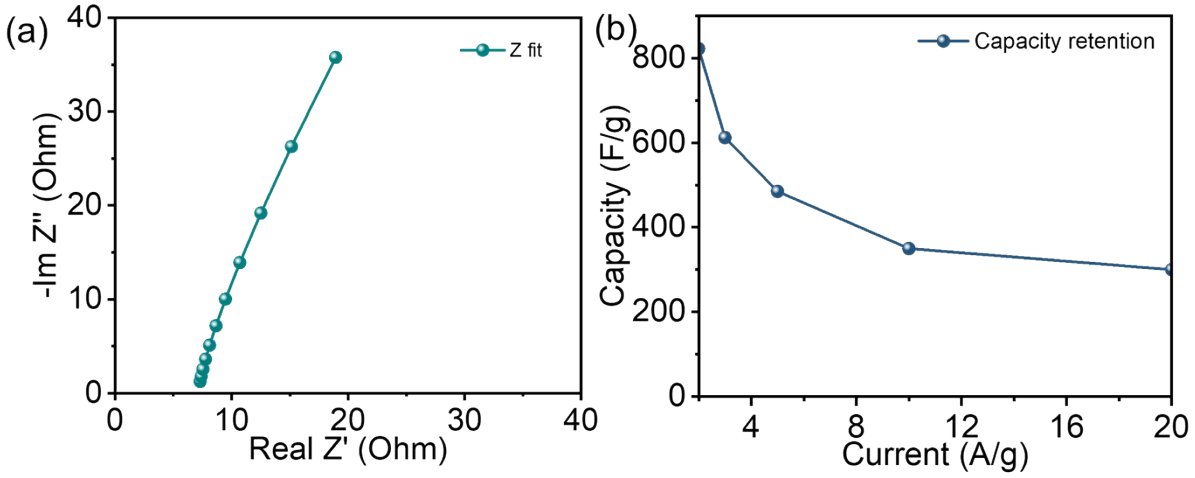

Figure S7. Electrochemical performance of PANI/VS_2 in the three-electrode system, (a) EIS impedance, and (b) capacity retention plot at the different current rates.

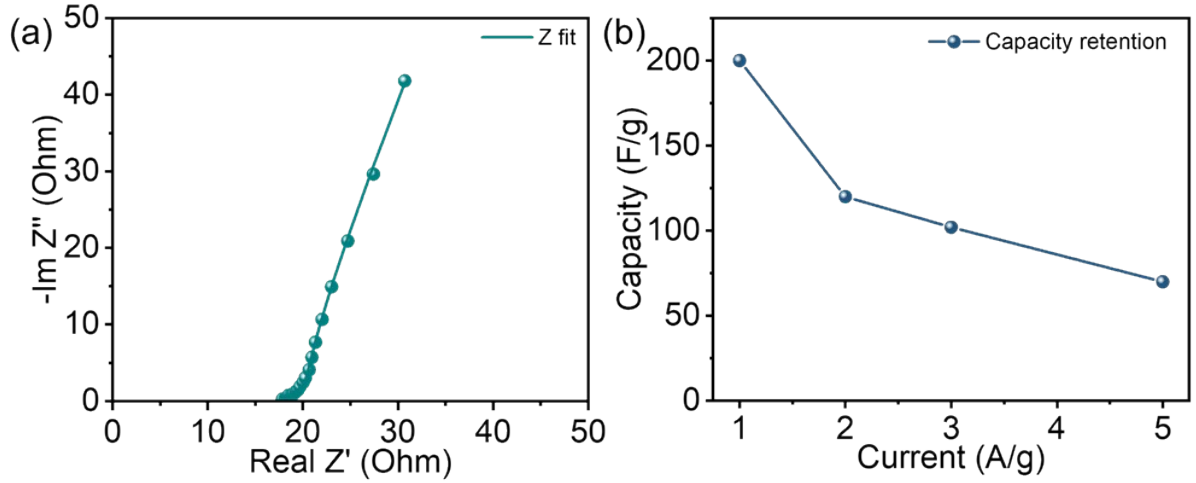

Figure S8. Electrochemical performance of PANI/VS_2 in the two-electrode system, (a) EIS impedance, and (b) capacity retention plot at the different current rates.

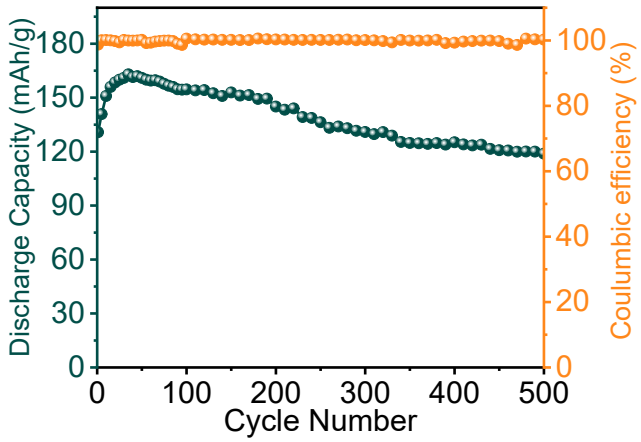

Figure S9. Cycling stability data recorded at the GCD current rate of 0.5 A g^{-1}.

Table 1. Summary of features of various cathode materials in aqueous ZIBs, such as energy storage mechanisms, testing voltage, discharge capacity, and electrolyte components

Cathode material	Reaction mechanism	Testing voltage (V)	Discharge capacity	Electrolyte components	Reference
α–MnO_2	Zn^{2+} insertion/extraction	0.7-2.0	210 $mAhg^{-1}$ (21 mAg^{-1})	1 M $ZnSO_4$	1
α–MnO_2	Zn^{2+} insertion/extraction	1.0-1.9	210 $mAhg^{-1}$ (0.5 C)	$Zn(NO_3)_2$	2
β–MnO_2	Zn^{2+} insertion/extraction	0.8-1.9	307 $mAhg^{-1}$ (0.32 C)	3 M $Zn(CF_3SO_3)_2$	3
$ZnMn_2O_4$	Zn^{2+} insertion/extraction	0.8-2.0	150 $mAhg^{-1}$ (50 mAg^{-1})	3 M $Zn(CF_3SO_3)_2$	4
Mn_3O_4	Zn^{2+} insertion/extraction	0.8-1.9	239.2 $mAhg^{-1}$ (100 mAg^{-1})	2 M $ZnSO_4$	5
$FeFe(CN)_6$	Zn^{2+} insertion/extraction	1.0-2.0	112 $mAhg^{-1}$ (10 mAg^{-1})	1.0 M $Zn(OAc)_2$ in [Ch]OAc + water	6
$Zn_3V_2O_7(OH)_2.2H_2O$	Zn^{2+} insertion/extraction	0.2-1.8	213 $mAhg^{-1}$ (50 mAg^{-1})	1 M $ZnSO_4$	7
$Na_3V_2(PO_4)_2F_3$	Zn^{2+} insertion/extraction	0.8-1.9	64.7 $mAhg^{-1}$ (80 mAg^{-1})	2 M $Zn(CF_3SO_3)_2$	8
PANI/VS_2	H^+ /Zn^{2+} insertion/ extraction	0.4-1.9	219 $mAhg^{-1}$ (100 mAg^{-1})	1 M $Zn(CF_3SO_3)_2$	**Our work**

Supplementary video S1. Demonstration of ZIB by emitting the SNIoE logo using 36 red LED bulbs of 3 V connected in parallel (at 3x speed).

References

1. Lee, B.; Yoon, C. S.; Lee, H. R.; Chung, K. Y.; Cho, B. W.; Oh, S. H. Electrochemically-Induced Reversible Transition from the Tunneled to Layered Polymorphs of Manganese Dioxide. *Sci. Rep.* **2015**, 4, 6066.
2. Xu, C.; Li, B.; Du, H.; Kang, F. Energetic zinc ion chemistry: the Rechargeable Zinc Ion Battery. *Angew. Chem., Int. Ed.* **2012,** 51, 933−5.
3. Zhang, N.; Cheng, F.; Liu, J.; Wang, L.; Long, X.; Liu, X.; Li, F.; Chen, J. Rechargeable Aqueous Zinc-Manganese Dioxide Batteries with High Energy and Power Densities. *Nat. Commun.* **2017,** 8, 405.
4. Zhang, N.; Cheng, F.; Liu, Y.; Zhao, Q.; Lei, K.; Chen, C.; Liu, X.; Chen, J. Cation-Deficient Spinel $ZnMn_2O_4$ Cathode in Zn-$(CF_3SO_3)_2$ Electrolyte for Rechargeable Aqueous Zn-Ion Battery. *J. Am. Chem. Soc.* **2016,** 138, 12894−12901.
5. Hao, J. W.; Mou, J.; Zhang, J. W.; Dong, L. B.; Liu, W. B.; Xu, C. J.; Kang, F. Y. Electrochemically Induced Spinel-Layered Phase Transition of Mn_3O_4 in High Performance Neutral Aqueous Rechargeable Zinc Battery. *Electrochim. Acta* **2018,** 259, 170−178.
6. Liu, Z.; Pulletikurthi, G.; Endres, F. A Prussian Blue/Zinc Secondary Battery with a Bio-Ionic Liquid-Water Mixture as Electrolyte. *ACS Appl. Mater. Interfaces* **2016,** 8, 12158−64.
7. Xia, C.; Guo, J.; Lei, Y.; Liang, H.; Zhao, C.; Alshareef, H. N. Rechargeable Aqueous Zinc-Ion Battery Based on Porous Framework Zinc Pyrovanadate Intercalation Cathode. *Adv. Mater.* **2018,** 30, 1705580.
8. Li, W.; Wang, K.; Cheng, S.; Jiang, K. A Long-Life Aqueous Zn-Ion Battery Based on $Na_3V_2(PO_4)_2F_3$ Cathode. *Energy Storage Mater.* **2018,** 15, 14−21.